Precipitation growth of graphene under exfoliated hexagonal boron nitride to form heterostructures on cobalt substrate by molecular beam epitaxy

Renjing Zheng, Alireza Khanaki, Hao Tian, Yanwei He, Yongtao Cui, Zhongguang Xu, and Jianlin Liu

Citation: Appl. Phys. Lett. **111**, 011903 (2017); doi: 10.1063/1.4991369
View online: http://dx.doi.org/10.1063/1.4991369
View Table of Contents: http://aip.scitation.org/toc/apl/111/1
Published by the American Institute of Physics

Precipitation growth of graphene under exfoliated hexagonal boron nitride to form heterostructures on cobalt substrate by molecular beam epitaxy

Renjing Zheng,[1] Alireza Khanaki,[1] Hao Tian,[1] Yanwei He,[1] Yongtao Cui,[2] Zhongguang Xu,[1] and Jianlin Liu[1,a)]
[1]*Quantum Structures Laboratory, Department of Electrical and Computer Engineering, University of California, Riverside, California 92521, USA*
[2]*Department of Physics and Astronomy, University of California, Riverside, California 92521, USA*

(Received 1 May 2017; accepted 20 June 2017; published online 5 July 2017)

Research on graphene/hexagonal boron nitride (h-BN) heterostructures has attracted much attention for band engineering and device performance optimization of graphene. However, the growth of graphene/h-BN heterostructure is still challenging, which usually requires high growth temperature and long growth duration. In this paper, we demonstrate graphene/h-BN heterostructures by growing graphene onto the substrates which consist of exfoliated h-BN flakes on Co thin films using molecular beam epitaxy. The heterostructure samples grown at different temperatures and growth times were characterized by Raman, optical microscopy, atomic force microscopy, microwave impedance microscopy, and scanning tunneling microscopy. It is found that the graphene/h-BN heterostructures were formed by the formation of graphene underneath rather than on top of the h-BN flakes. The growth mechanism is discussed. *Published by AIP Publishing.*
[http://dx.doi.org/10.1063/1.4991369]

Graphene and hexagonal boron nitride (h-BN) are van der Waals (vdW) materials, and they share the same layered crystal structure and hexagonal symmetry, with a small lattice mismatch of only ~1.7%. Graphene/h-BN heterostructures have a great deal of potential applications in diverse areas, including photo-electricity,[1–4] catalysts,[5] and transistors,[6–10] which stimulate tremendous effort on the synthesis and characterization of the heterostructures containing graphene and h-BN. Much work has been reported about the preparation of the heterostructures by employing different growth methods and using different substrates.[11–18] However, the realization of epitaxial heterostructures (graphene on h-BN or h-BN on graphene) remains challenging. Because of the stability of boron atoms and nitrogen molecules under inert conditions, the reaction to form h-BN usually requires high growth temperature (GT) (>900 °C) and long growth duration (several hours).[19–23] Additionally, due to the weak vdW interaction, it is difficult for boron and nitrogen atoms to stick on to the surface of a deposited film, thus hindering the growth of h-BN films with a controllable thickness for dielectric materials and barriers.

In this paper, we demonstrate a pathway to produce graphene/h-BN heterostructures. By introducing C_2H_2 gas molecules onto the heated exfoliated h-BN flake covered cobalt (Co) substrate in a molecular beam epitaxy (MBE) system, we observed that instead of layer-by-layer growth of graphene on top of h-BN, the carbon atoms dissolve in Co, diffuse, and grow underneath h-BN flakes by precipitation to form graphene/h-BN heterostructures. Various methods were employed to characterize the samples. Growth mechanism involving the dissolution/diffusion/precipitation of carbon atoms in Co is discussed.

A 300-nm Co thin film was grown on a SiO_2/Si wafer by an e-beam evaporator. After that, h-BN flakes were transferred on Co by the tape-exfoliation method to finish substrate preparation.[24] The substrates were subsequently transferred to a Perkin-Elmer MBE chamber for graphene growth. Acetylene gas (C_2H_2, Airgas, 99.9999%) was connected to the MBE chamber as C source, while H_2 gas (Airgas, 99.9999%) was also introduced into the chamber through a needle valve before and during the growth. The substrate temperature was ramped to a target growth temperature between 720 °C and 800 °C with a ramping rate of 10 °C/min. Before the growth, the substrate was annealed in 10-sccm H_2 for 10 min to remove possible contamination. Then, the H_2 flow rate was decreased to 6 sccm, and graphene growth started by the introduction of 3-sccm acetylene. The growth duration lasted from 60 to 1200 s for different samples. After the growth, the sample was cooled to room temperature with a cooling rate of 10 °C/min.

The surface roughness of the substrate was measured by a tapping mode Veeco D5000 atomic force microscopy (AFM) system. Optical microscopy and Raman characterizations were performed using a HORIBA LabRam system equipped with a 60-mW 532-nm green laser. A lab-built microwave impedance microscope (MIM) based on a contact-mode Bruker Dimension Icon AFM platform was used for surface morphology and conductance analysis of samples. The samples were also studied using a Nanosurf Naio scanning tunneling microscope (STM).

Before the growth, AFM characterization was performed on prepared exfoliated h-BN flakes on the Co thin film substrate [Fig. 1(a)]. H-BN flakes are less in density on Co than that on the SiO_2/Si substrate using the same procedure, which is due to rougher Co surface [root mean square (RMS) roughness is ~1.5 nm at 4 μm^2 area]. The Raman spectrum [Fig. 1(a)] shows a sharp h-BN E_{2g} peak located at

a)Author to whom correspondence should be addressed: jianlin@ece.ucr.edu. Tel.: 1-9518277131. Fax: 1-9518272425.

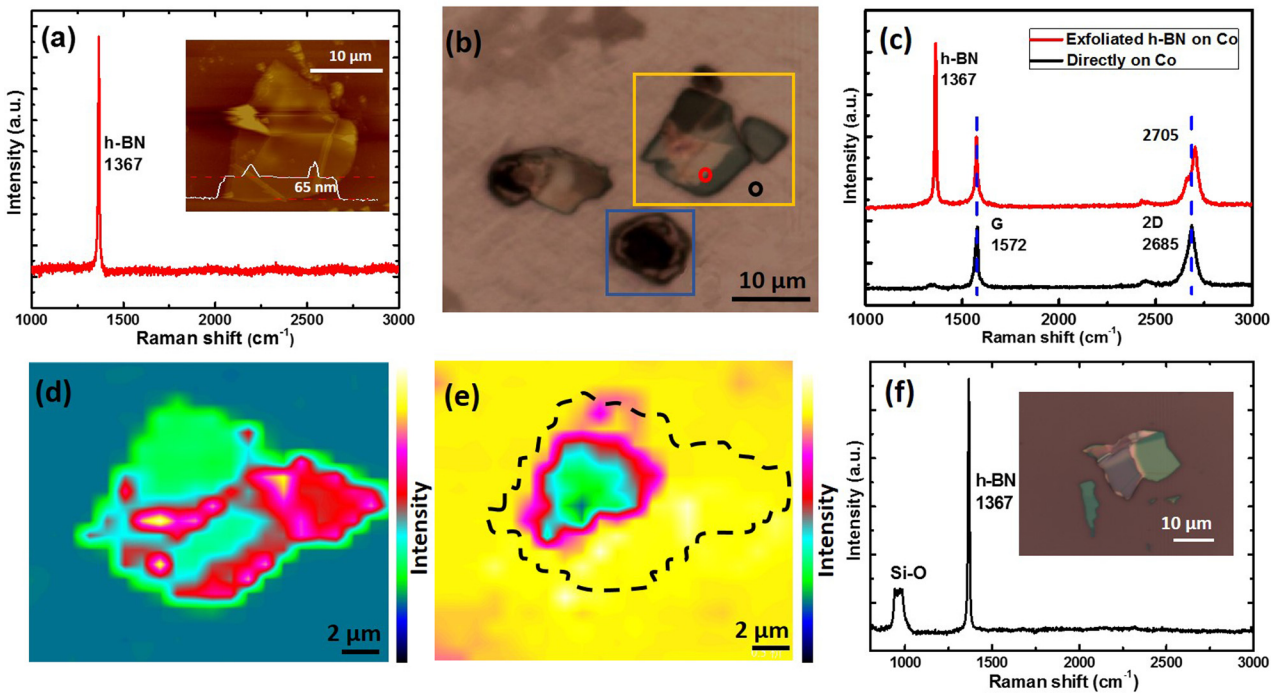

FIG. 1. Characterizations of an as grown graphene/exfoliated h-BN heterostructure. (a) Raman spectrum of a typical exfoliated h-BN flake on Co substrate. The inset is an AFM image of the substrate. (b) Optical microscopy image of an as grown sample, which was grown at 740 °C for 100 s. Yellow square and blue square are marked on the image to indicate the h-BN flake and heat-induced hole, respectively. (c) Raman spectra of as-grown sample, which are measured on the part shown in the red and black circles in (b). (d), (e) Raman mapping of h-BN E_{2g} and graphene G peaks. The mapping area is within the yellow square indicated in (b). (f) Raman spectrum and inset optical microscopy image of a reference sample grown at the same growth condition on a substrate with exfoliated h-BN directly on SiO_2.

1367 cm^{-1} for a flake of ~100 μm^2 and a thickness of ~65 nm. The RMS roughness of h-BN at the center area is 0.85 nm (4 μm^2 area), and some "wrinkles" on the h-BN are also observed in the AFM image. A typical growth was done at 770 °C for 100 s. From the optical microscopy image of this sample [Fig. 1(b)], two h-BN flakes can be found and a hole is formed in the Co film (blue square), which is due to partial evaporation of Co at high temperature. Most surface area of Co shows uniform color contrast except some parts especially on the top left corner, which means graphene is locally uniform. The red and black Raman spectra as shown in Fig. 1(c) were obtained on and away from the h-BN flake, respectively, corresponding to the areas marked by the red and black circles in Fig. 1(b). The black Raman spectrum shows clear graphene Raman G and 2D peaks at 1572 and 2685 cm^{-1}, respectively, with a G/2D peak intensity ratio of ~1. This indicates the existence of bi- or tri-layer graphene on the exposed Co film area. When the measurement was done on the h-BN flake, h-BN E_{2g}, graphene G and 2D peaks are revealed. In addition, a 20-cm^{-1} blue shift of the 2D peak is found, which is discussed further in Fig. 3. Detailed Raman mapping of h-BN E_{2g} and graphene G peaks was performed, and the results are shown in Figs. 1(d) and 1(e), respectively. The mapping area is shown by the yellow square in Fig. 1(b). The H-BN flake shape is identified in Fig. 1(d), which agrees with the optical microscopy image. Different intensities are observed because of different thicknesses of h-BN layers from the exfoliation process. A more uniform color distribution in Fig. 1(e) shows the graphene film coverage. However, weaker or even no graphene signal can be observed in the center part of the h-BN flake (dashed line area). The distribution is not correlated with the thickness or roughness of the h-BN flake but relies on the size of the h-BN flake and diffusivity of carbon atoms in Co. The Raman characterization of the area with a smaller h-BN flake shows that graphene coverage is full and uniform under the entire flake, further proving this point (Fig. S1 in the supplementary material). For comparison, a reference sample was grown on a substrate having exfoliated h-BN flakes on SiO_2/Si using the same conditions [Fig. 1(f)]. No graphene signal can be detected, which implies the importance of Co. The importance of Co on the growth of graphene is further confirmed by the growth and characterization of a sample on a substrate with exfoliated h-BN partially covering heat-induced holes in the Co thin film (Fig. S2 in the supplementary material).

Our previous results reveal that the GT has a significant impact on the characteristics of graphene films on iron substrates.[25] Here, besides the sample grown at 770 °C (Fig. 1), we tried other GTs: 800, 740, and 720 °C. Optical microscopy images show different graphene contrast in Figs. 2(a)–2(c). Thicker graphene regions (darker spots) with higher density are observed in the samples grown at higher GTs. Raman spectra were measured at the locations marked with red and black circles in the optical microscopy images. Sharp h-BN peaks are observed from all three samples. However, the graphene signal becomes weaker with the decrease in GT, and as the growth occurs at 720 °C, a visible D peak appears in the Raman spectrum, and the graphene signal is negligible when measured on the h-BN area. The situation that lower GT leads to weaker graphene signal happens on both bare Co and h-BN regions, which agrees with the optical microscopy observations.

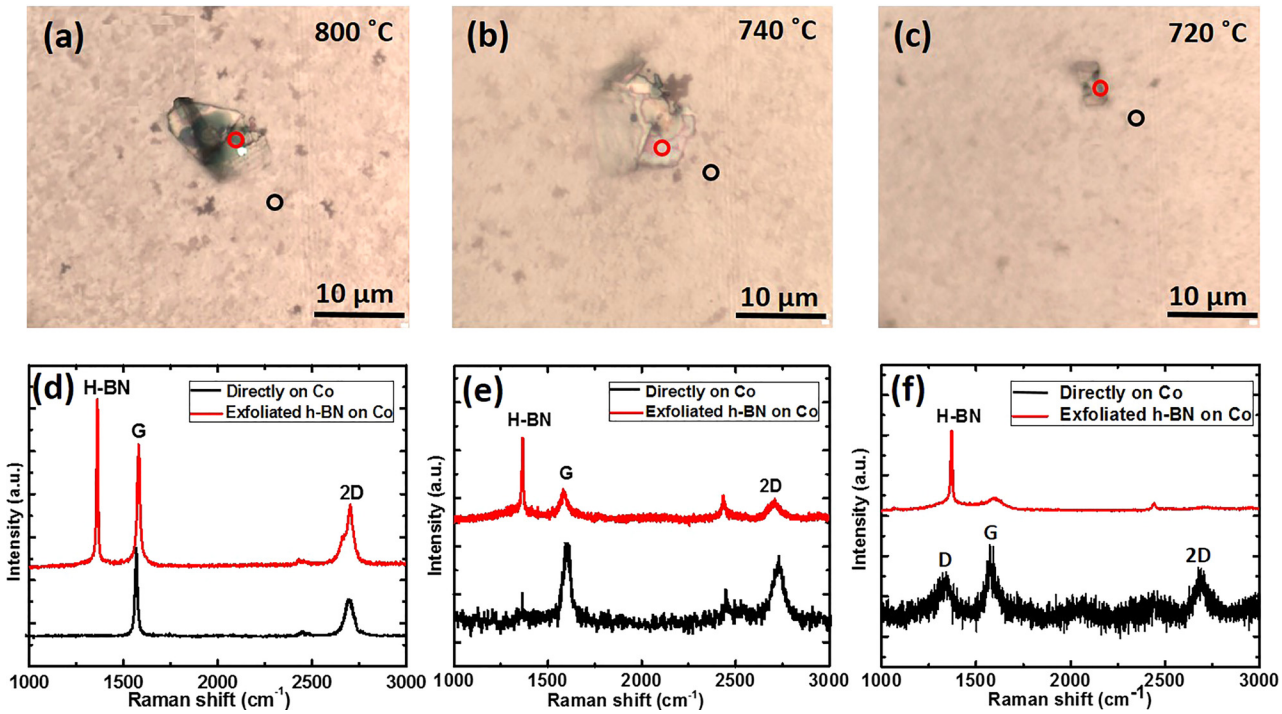

FIG. 2. Temperature-dependent graphene growth on exfoliated h-BN on Co. (a)–(c) Optical microscopy images of samples with graphene grown on exfoliated h-BN on Co, at a growth temperature of 800, 740, and 720 °C, respectively. (d)–(f) Raman spectra measured at locations indicated as red and black circles shown in (a)–(c).

Different samples were grown on exfoliated h-BN on Co at 770 °C with growth duration varying from 60 to 1200 s. Here, we present Raman spectra [Figs. 3(a)–3(c)] and optical microscopy images [Figs. 3(d)–3(f)] of samples grown at 60, 300, and 600 s, respectively. When the growth time is short (≤60 s), no graphene signal can be observed; and as the growth time increases, G peak appears and becomes larger, which means that graphene starts to grow. The same conclusion can be drawn from optical microscopy images. With longer growth time, more black domains are observed because of thicker graphene flakes. The graphene thickness dependence on the growth time is shown in Fig. 3(b). Assuming the thickness of h-BN flakes is roughly the same, we use the G/h-BN peak intensity ratio to identify the graphene thickness. With

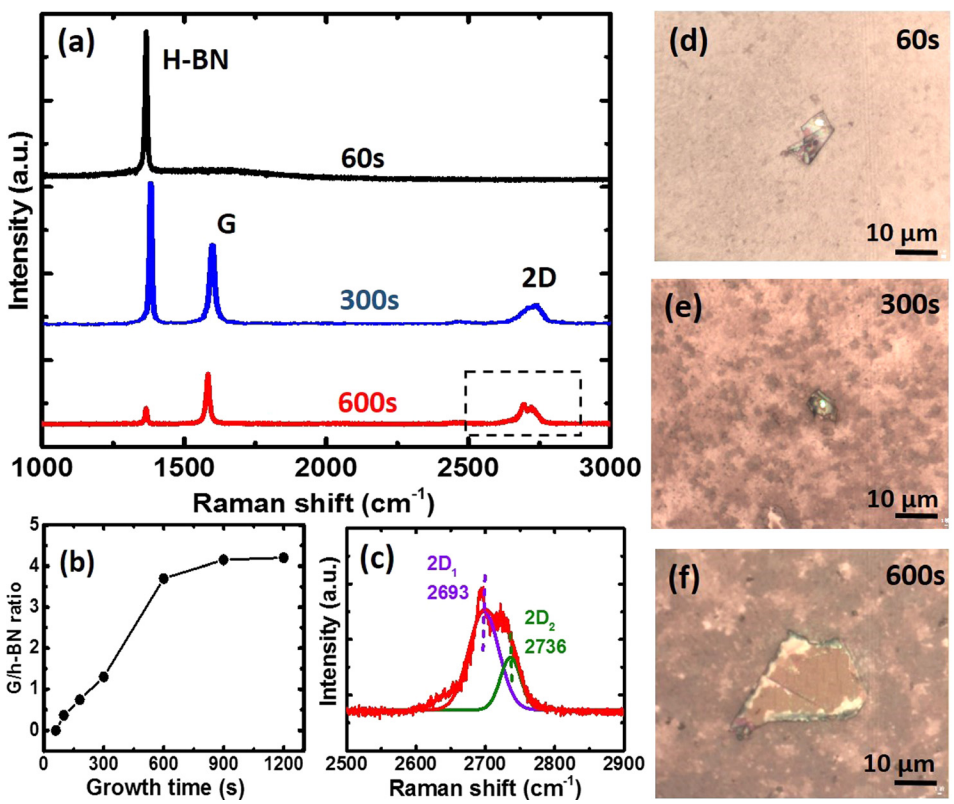

FIG. 3. Time-dependent graphene growth on exfoliated h-BN on Co. (a) Raman spectra of samples with growth duration varying from 60 to 600 s. The measurement was done in the exfoliated h-BN region. (b) the G/h-BN ratio as a function of growth time. (c) The zoomed-in Raman spectrum showing two components of graphene 2D peak at around 2700 cm^{-1}. (d)–(f) Optical microscopy images of samples grown for 60, 300, and 600 s, respectively.

the increase in the growth time, the graphene thickness increases; however, it reaches the saturation level after a long growth duration (≥900 s). This suggests that the graphene might not be epitaxially grown on top of h-BN; instead, it was formed by the precipitation of carbon from the Co substrate. The graphene thickness saturation under long growth time may be originated from carbon solubility in Co at certain temperature. As growth time is short, carbon solubility has not reached its saturation. With the increase in the growth time, more carbon atoms dissolve into the metal and subsequently form graphene. However, further increase in the growth time leads to the saturation of carbon atoms in Co. Thus, the resulting graphene thickness appears to be the same among these carbon-saturated samples due to the same cooling condition for the precipitation growth. Figure 3(c) shows the Raman spectrum near 2700 cm^{-1} of the sample grown for 600 s. After fitting, two peaks are found to exist at 2693 and 2736 cm^{-1}, which are the two components of graphene 2D peak.[26] Similar broaden 2D peaks have been observed for all heterostructure samples, which is due to the orientation and stacking of multilayer graphene.

A series of scanning probe microscopy (SPM) measurements were performed to further reveal that graphene grows underneath rather than on top of the exfoliated h-BN flake. Figure 4 summarizes the results from a sample grown at 770 °C for 100 s. An h-BN flake with a thickness of ~60 nm is observed by the contact mode AFM [Fig. 4(a)]. The roughness of the flake is around 0.90 nm for 4 μm^2 area, which is close to the RMS roughness value before growth. STM was performed to check the atomic information of the as-grown sample: a typical graphene STM pattern with a lattice constant of 2.40 Å is observed on Co [Fig. 4(b)], but no graphene signal is detected when measured on exfoliated h-BN [Fig. 4(c)]. This result implies that either there is completely no graphene or graphene is not continuous on top of insulating h-BN, leading to the difficulty to be detected. To clarify the situation, MIM measurement was carried out using a lab-built MIM system[27,28] with a solid platinum cantilever probe that has a sharp tip at the end. A microwave signal at 1 GHz was sent to the metal probe, and the reflection signal, determined by the tip-sample admittance (inverse of impedance) was analyzed [Fig. 4(d)]. When the tip makes direct electrical contact with a conductive region, a large increase in the MIM signal, referenced to the case when contacting an insulating region, can be detected. It is worth noting that the MIM detection of metallic regions does not require a back-electrode on the sample because MIM senses the local screening of the microwave electric field by the sample. In the simultaneously obtained MIM image, qualitatively different features are observed in the h-BN region and in its surrounding Co area: random spark signals (bright spots) are observed in the Co area, whereas the h-BN area has a consistently low MIM signal. The inhomogeneous MIM spark signals over the Co area is due to the imperfection of graphene quality and substrate flatness (the MIM image of pristine exfoliated graphene on SiO_2 is given in Fig. S3 in the supplementary material). In contrast, no sparks being detected in the h-BN area indicate that there is no graphene on top of h-BN. Since Raman spectra indicate the existence of graphene from the h-BN area, it can be concluded that graphene has not been grown on top of the exfoliated h-BN, but underneath the flake.

Further film transfer experiment was performed to remove the Co substrate of the sample grown at 770 °C for 100 s, and both h-BN and graphene signals are still detected after transferring (Fig. S4 in the supplementary material). It suggests that the vdW attractive force between as grown graphene and exfoliated h-BN can withstand the transferring process. This is a direct proof that the precipitation growth of graphene under the exfoliated h-BN layers undergoes the vdW growth mode.

Finally, we can briefly discuss the growth mechanism as illustrated in Fig. 4(f). C_2H_2 decomposes into carbon and hydrocarbon atoms on the Co surface, and the dissolved carbon atoms diffuse into the area under the exfoliated h-BN flake and precipitate later in the same area to form graphene during the substrate cooling period. As grown graphene attaches to the bottom surface of the exfoliated h-BN through vdW forces. The graphene coverage underneath h-BN is determined by the carbon solubility in Co, diffusion length

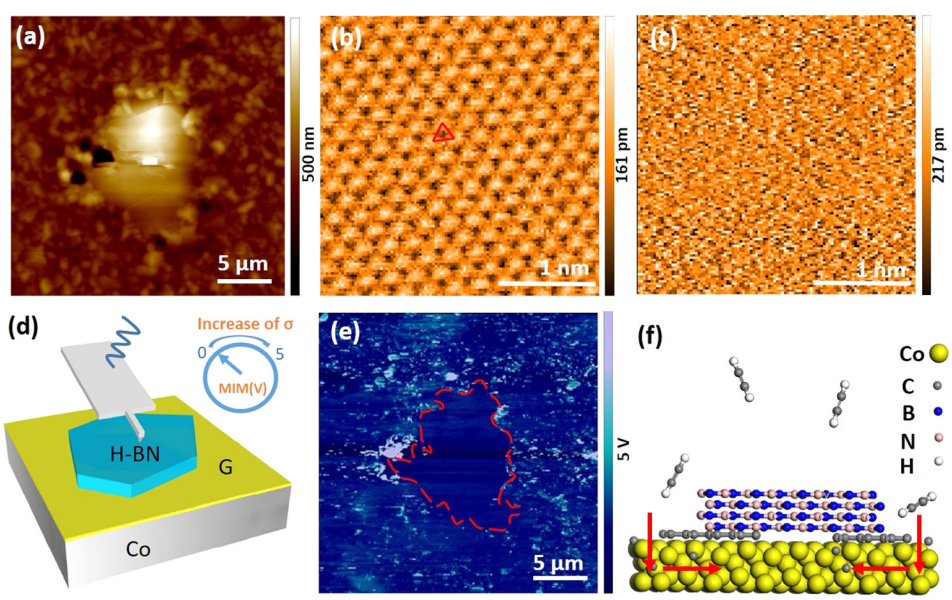

FIG. 4. SPM images of an as-grown graphene/exfoliated h-BN heterostructure sample. (a) AFM image of the as-grown sample. (b), (c) STM images of the as-grown sample, on Co and in h-BN region, respectively. (d) Illustration of lab-built AFM-based MIM setup. (e) MIM image of the sample area shown in (a), the dashed line indicates the h-BN area. (f) Schematic growth mode of graphene on exfoliated h-BN on Co.

(how far carbon atoms can reach the center area of h-BN from its edge), and substrate temperature cooling rate. It should be noted that although Co is selected here to demonstrate the heterostructure formation mechanism of epitaxial graphene under exfoliated h-BN, other parameters such as the thickness of Co, substrate cooling rate, and other metal substrates can be chosen to further control the number of graphene layers. For example, we may prepare a substrate by transferring exfoliated h-BN onto Cu-Ni alloy and perform similar growth to achieve single- or bi-layer graphene under the h-BN with controlling the fraction of Ni.[29,30] These future efforts will certainly enrich graphene/h-BN heterostructures for various applications.

In summary, we demonstrated the h-BN/graphene heterostructure by precipitation growth of graphene under exfoliated h-BN flakes on Co film substrates. The growth was done by introducing C_2H_2 gas onto the heated substrate in an MBE chamber. No graphene was grown on top of the h-BN flakes under the investigated growth conditions. The graphene coverage and thickness are dependent on the size of h-BN flakes, growth temperature, and duration, which is related to the carbon's diffusion length and solubility in Co. This growth method provides a convenient path to produce graphene/h-BN heterostructures, which avoids high temperature and long duration needed for BN growth.

See supplementary material for the optical microscopy and Raman scattering characterization of graphene on smaller-size exfoliated h-BN on Co, graphene on h-BN on Co with heat-induced holes and a transferred graphene/h-BN heterostructure sample, and AFM/MIM studies of pristine graphene reference sample.

This work was supported by FAME, one of six centers of STARnet, a Semiconductor Research Corporation program supported by MACRO and DARPA.

[1]K. Kim, J. Y. Choi, T. Kim, S. H. Cho, and H. J. Chung, Nature **479**, 338 (2011).
[2]A. Kumar, T. Low, K. H. Fung, P. Avouris, and N. X. Fang, Nano Lett. **15**, 3172 (2015).
[3]M. B. Lundeberg, Y. Gao, A. Woessner, C. Tan, P. Alonso-González, K. Watanabe, T. Taniguchi, J. Hone, R. Hillenbrand, and F. H. Koppens, Nat. Mater. **16**, 204 (2017).
[4]Y. Lu, Z. Wu, W. Xu, and S. Lin, Nanotechnology **27**, 48LT03 (2016).
[5]Y. Zheng, Y. Jiao, L. Ge, M. Jaroniec, and S. Z. Qiao, Angew. Chem. **125**, 3192 (2013).
[6]L. Britnell, R. V. Gorbachev, R. Jalil, B. D. Belle, F. Schedin, A. Mishchenko, and T. Georgiou, Science **335**, 947 (2012).
[7]G. H. Lee, Y. J. Yu, X. Cui, N. Petrone, C. H. Lee, M. S. Choi, and D. Y. Lee, ACS Nano **7**, 7931 (2013).
[8]C. Kumar, M. Kuiri, J. Jung, T. Das, and A. Das, Nano Lett. **16**, 1042 (2016).
[9]L. Britnell, R. V. Gorbachev, A. K. Geim, L. A. Ponomarenko, A. Mishchenko, M. T. Greenaway, T. M. Fromhold, K. S. Novoselov, and L. Eaves, Nat. Commun. **4**, 1794 (2013).
[10]E. Vdovin, A. Mishchenko, M. T. Greenaway, M. J. Zhu, D. Ghazaryan, A. Misra, and Y. Cao, Phys. Rev. Lett. **116**, 186603 (2016).
[11]M. Drögeler, F. Volmer, M. Wolter, B. Terrés, K. Watanabe, T. Taniguchi, G. Güntherodt, C. Stampfer, and B. Beschoten, Nano Lett. **14**, 6050 (2014).
[12]S. M. Kim, A. Hsu, P. T. Araujo, Y. H. Lee, T. Palacios, M. Dresselhaus, J. C. Idrobo, K. K. Kim, and J. Kong, Nano Lett. **13**, 933 (2013).
[13]Z. Zuo, Z. Xu, R. Zheng, A. Khanaki, J. G. Zheng, and J. Liu, Sci. Rep. **5**, 14760 (2015).
[14]Z. Xu, R. Zheng, A. Khanaki, Z. Zuo, and J. Liu, Appl. Phys. Lett. **107**, 213103 (2015).
[15]L. Banszerus, M. Schmitz, S. Engels, J. Dauber, M. Oellers, F. Haupt, K. Watanabe, T. Taniguchi, B. Beschoten, and C. Stampfer, Sci. Adv. **1**, e1500222 (2015).
[16]C. Zhang, S. Zhao, C. Jin, A. L. Koh, Y. Zhou, W. Xu, Q. Li, Q. Xiong, H. Peng, and Z. Liu, Nat. Commun. **6**, 6519 (2015).
[17]I. Meric, C. R. Dean, N. Petrone, L. Wang, J. Hone, P. Kim, and K. L. Shepard, Proc. IEEE **101**, 1609 (2013).
[18]Z. Xu, H. Tian, A. Khanaki, R. Zheng, M. Suja, and J. Liu, Sci. Rep. **7**, 43100 (2017).
[19]G. H. Han, J. A. Rodríguez-Manzo, C. W. Lee, N. J. Kybert, M. B. Lerner, Z. J. Qi, E. N. Dattoli, A. M. Rappe, M. Drndic, and A. T. C. Johnson, ACS Nano **7**, 10129 (2013).
[20]H. Hibino, S. Wang, C. M. Orofeo, and H. Kageshima, Prog. Cryst. Growth Charact. Mater. **62**, 155 (2016).
[21]J. M. Wofford, S. Nakhaie, T. Krause, X. Liu, M. Ramsteiner, M. Hanke, H. Riechert, and J. M. J. Lopes, Sci. Rep. **7**, 43644 (2017).
[22]Z. Xu, A. Khanaki, H. Tian, R. Zheng, M. Suja, J. G. Zheng, and J. Liu, Appl. Phys. Lett. **109**, 043110 (2016).
[23]Y. Yang, Q. Fu, H. Li, M. Wei, J. Xiao, W. Wei, and X. Bao, ACS Nano **9**, 11589 (2015).
[24]D. Pacile, J. C. Meyer, Ç. Ö. Girit, and A. Zettl, Appl. Phys. Lett. **92**, 133107 (2008).
[25]R. Zheng, Z. Xu, A. Khanaki, H. Tian, Z. Zuo, J.-G. Zheng, and J. Liu, Thin Solid Films **627**, 39 (2017).
[26]A. C. Ferrari and D. M. Basko, Nat. Nanotechnol. **8**, 235 (2013).
[27]W. Kundhikanjana, K. Lai, H. Wang, H. Dai, M. A. Kelly, and Z. X. Shen, Nano Lett. **9**, 3762 (2009).
[28]Z. Wei, E. Y. Ma, Y. T. Cui, S. Johnston, Y. Yang, K. Agarwal, M. A. Kelly, Z. X. Shen, and X. Chen, Rev. Sci. Instrum. **87**, 094701 (2016).
[29]X. Liu, L. Fu, N. Liu, T. Gao, Y. Zhang, L. Liao, and Z. Liu, J. Phys. Chem. C **115**, 11976 (2011).
[30]S. Chen, W. Cai, R. D. Piner, J. W. Suk, Y. Wu, Y. Ren, J. Kang, and R. S. Ruoff, Nano Lett. **11**, 3519 (2011).